Journal of Magnetic Resonance **142,** 382–385 (2000)
doi:10.1006/jmre.1999.1949, available online at http://www.idealibrary.com on IDEAL®

Three-Dimensional Pulsed ESR Fourier Imaging

A. Feintuch, G. Alexandrowicz, T. Tashma, Y. Boasson, A. Grayevsky, and N. Kaplan

Racah Institute of Physics, Hebrew University of Jerusalem, Jerusalem 91904, Israel

Received July 21, 1999; revised September 27, 1999

Three-dimensional pulsed ESR imaging was performed on a $(FA)_2PF_6$ crystal using a three-dimensional Fourier imaging sequence. The best resolution achieved was of 20 μm^3. Comparison with images obtained using the filtered back-projection method shows the superiority of this method under the given conditions.

Key Words: **pulsed ESR; Fourier imaging; filtered back-projection.**

The first example of 3D ESR time domain imaging was reported recently by Coy *et al.* (*1*). By applying a low polarizing field they were able to avoid the microwave cavity and use standard RF methods. They used a filtered back-projection (FBP) pulse sequence and achieved a nominal spatial resolution of 34 μm^3 in an acquisition time of 12 h. The actual physical resolution was not verified. As detailed in (*1*) the FBP method was utilized, rather than the conventional spin warp Fourier imaging (FI), in order to avoid some of the technical difficulties involved in the implementation of the latter. Specifically, the imaging was performed on a $(FA)_2PF_6$ sample with a transverse ESR relaxation time of $T2 \approx 6$ μs. The FI method requires switching the gradient pulses on and off during the lifetime of the transverse magnetization, which for these samples would require switching times of submicroseconds. This feature is not available in conventional commercial linear current amplifiers. On the other hand, FI has numerous advantages over the FBP method, especially pertaining to $(FA)_2PF_6$ samples. A key feature of $(FA)_2PF_6$ is that electron diffusion is highly anisotropic. It has been shown that the self-diffusion coefficient is up to three orders of magnitude larger along the direction of the fluoranthene ring chains, compared with the diffusion perpendicular to the chains (*2*). Therefore, the Cartesian encoding of the sample utilized by the FI method enables better control over diffusion artifacts, compared with the spherical encoding used by FBP. Additionally, since the spatial encoding in FI is obtained through the use of short gradient pulses, diffusion effects are limited to the duration of the pulse, while encoding based on a static read gradient, such as utilized by FBP, is affected by diffusion during the entire "read" window. Another advantage of the FI method lies in the reconstruction procedure. Reconstruction in the FBP method involves interpolation from a spherical grid to a Cartesian grid, a procedure which could cause artifacts in the reconstructed image. In FI the reconstruction is done through a straightforward Fourier transform. In this Communication we report on the first example of 3D ESR time domain imaging which utilizes spatial phase encoding sequences.

The imaging was performed on a $(FA)_2PF_6$ sample, placed in the fringe field of a superconducting NMR magnet. This configuration was necessary to avoid effects of eddy currents due to rapidly switched gradient pulses as demonstrated earlier (*3*). A fringe field of 0.0106 T was used producing a conduction electron ESR signal at 300 MHz. A Tecmag NMR spectrometer operating at 300 MHz was used to perform the measurements. The imaging probe included RF coils of 1–2 mm diameter prepared individually for each sample and three gradient coils each producing 0.2 T m^{-1} A^{-1}. The gradient assembly was manufactured at Massey University, New Zealand. As mentioned previously, performing FI on this sample requires the ability to produce phase encoding gradient pulses with switching times of submicroseconds. The gradient pulses were produced by the use of a homebuilt pulsed current driver based on the "clipped L-C resonant circuit" idea of Conradi *et al.* (*4*). The driver produces pulses with a duration of 2.7 μs which can be repeated as fast as every 5 μs. Current drivers of this type were already used successfully in PGSE ESR experiments (*3*).

The more conventional approach to volume imaging, i.e., a multislice scheme, is not suitable for the present situation. The advantage of slice-selective excitation over the use of 3D imaging lies in the ability to limit the acquisition to a single slice, a feature which is not available in 3D FI. Therefore, when there is a priori interest only in a partial image of the volume, 3D FI is unnecessarily time consuming. However, this is correct only in situations where there is no need for many averaging steps to obtain a single slice. In situations where obtaining a single slice requires many averaging steps, such as in our sample, excitation of the whole volume in each phase encoding step requires less averaging than a single slice and therefore compensates for the time spent on phase encoding. Thus, the alternative we chose was to use three-dimensional Fourier imaging sequences.

In the presence of magnetic field gradients the relation between spin density and signal is given by

1090-7807/00 $35.00

$$\rho(x, y, z) = \int\int\int S(k_x, k_y, k_z) \times \exp(2\pi i(k_x x + k_y y + k_z z))dxdydz, \quad [1]$$

where k_x, k_y, and k_z are functions of the applied gradients (*5*). 3D FI is based on a Cartesian three-dimensional mapping of *k*-space. In principle, in order to minimize diffusion artifacts this mapping should be done by a three-dimensional phase encoding. As mentioned previously, in $(FA)_2PF_6$ electron diffusion is highly anisotropic, with very low diffusion perpendicular to the fluoranthene ring chains. For technical convenience, we therefore chose to map one of the perpendicular directions with a static read gradient. The positioning of the sample relative to the gradient coils axes was done with the use of a PGSE sequence (*6*). The sample was positioned such that the echo attenuation due to diffusion in a PGSE sequence would be maximal in one direction and minimal in the perpendicular directions. The directions which showed minimal attenuation were identified as perpendicular to the conduction chains.

To produce a N^3 image array using two phase gradients and a read gradient, it was necessary for us to perform N^2 independent acquisitions, each acquisition window containing N sampled points. The time therefore necessary to produce an image is dependent on N^3. Due to this dependency we chose to limit the size of the image array to 64^3, in order to minimize imaging time. To enable a minimal voxel size of 15 μm^3, this dictates a field of view of approximately 1 mm^3. Some of the samples we used therefore were with a long dimension of less than 1 mm, so that sample size did not limit the resolution. The sequence we used was a spin-echo sequence, with two pulsed phase gradients, both performed between the 90 and 180 RF pulses, and one static read gradient. The static gradient is turned on in advance and kept on during the entire acquisition of the image, to avoid switching time effects. Due to the duration of the phase encoding gradient pulses it was necessary to work with a relatively long echo time, 2τ, of 9 μs. An individual sequence required therefore approximately 7 μs before beginning the acquisition and 64×0.2 $\mu s = 12.8$ μs as an acquisition window. Because of some extra "system" time, the average sequence required approximately 28 μs. A typical sequence is presented in Fig. 1. Each acquisition consisted of 8 (phase cycled) inner averaging steps and 5000 outer signal averaging steps, leading to a total imaging time of 1.5 h for the 64^2 phase steps. Data transfer on our spectrometer is immediate. Due to receiver "dead" time of 2 μs following the RF pulse, the echo was only partially acquired, and reconstruction was done using a partial Fourier reconstruction algorithm (*7*). Acquisition of the whole echo is possible only for a longer τ and is therefore costly in terms of signal amplitude. The phase encoding was done by incrementing the amplitude of the pulsed gradients during $64 * 64$ independent acquisitions,

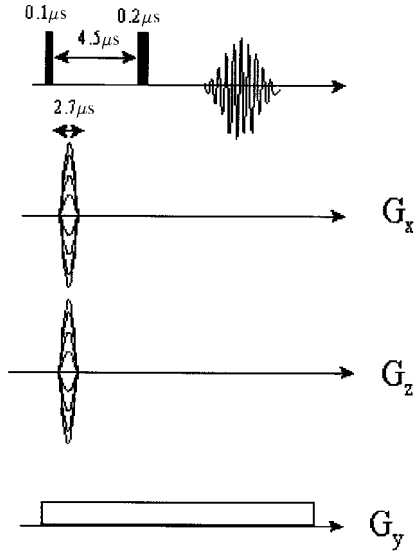

FIG. 1. A typical ESR FI sequence.

while the pulse duration remained constant. For a given gradient amplitude the coordinate in *k*-space will be given by $k = \gamma/2\pi \int_{\delta t} G dt$ where the integration is on the pulse duration. The relation between voxel size and the maximal gradient amplitude is given by $\Delta x = 1/(2 * k_{max})$, therefore, to achieve a resolution of 30 μm we applied a gradient such that $k_{max} = 1.6 * 10^4$ m^{-1}.

In clinical MRI systems imaging artifacts are characterized through the use of phantoms with well-defined inner and outer structure. The crystal growing procedure of the $(FA)_2PF_6$ samples we are currently imaging does not enable us to create such conditions. It is therefore necessary to use different methods to verify the authenticity of the images obtained. Optical microscopy can be used to verify the outer structure, but it is not useful for identifying inner features. A partial verification of inner features can be achieved by repeating the same imaging procedure with the sample rotated at different angles with respect to the imaging axes and comparing the results. In Fig. 2 we present two slices of the sample in the *y*-*z* plane, obtained at two different angles around the *x* axis, with a resolution of 30 μm^3. It is clear that the fracture observed in the center of the sample has been rotated together with the sample and is similar in both images. This fracture is also visible in the *x*-*y* and *x*-*z* planes presented in Fig. 3. An image of the same sample, obtained through the FBP method (implemented on the basis of Coy *et al.* (*1*)), using 669 different projections, is presented in Fig. 4. Although the outer structure displayed by both methods is similar, the inner features are only partially discernible due to apparent smearing artifacts. The absence of such smearing from the FI image indicates that it might be related to diffusion-limited resolution effects (*9*). As mentioned previously, the FI image was acquired with the read gradient oriented carefully perpendicular to the conducting channels in the sample. Thus we minimized the gradient component along the

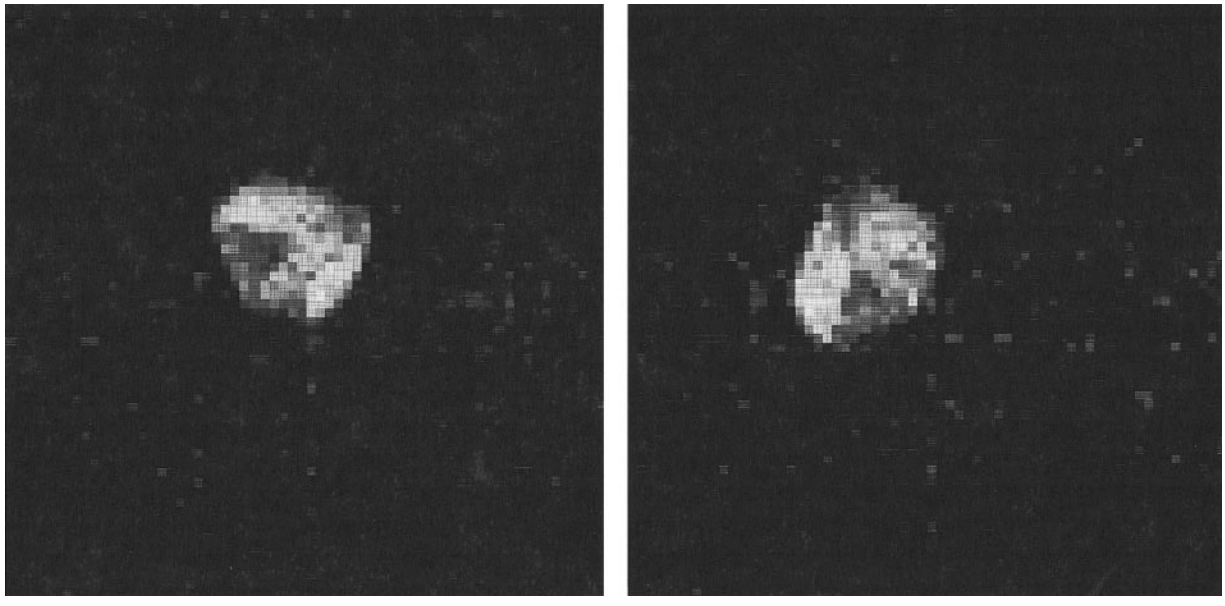

FIG. 2. Slices of the *y*-*z* plane at two different sample positions, reconstructed from 3D FI acquisition data of $(FA)_2PF_6$. The voxel size is 30 μm^3 giving a total fov of 1.9 mm^3.

chains during the read window and therefore minimized signal attenuation and spectral spread due to diffusion. Since the read gradient in the FBP scheme is applied along all angular directions, most of the read acquisitions are performed with a significant gradient component along the conducting channels. This could lead to the aforementioned diffusion-limited resolution phenomenon. Another explanation could be that the smearing is related to the uneven sampling of *k*-space in the back-projection method. Since the finer details of an image are represented in *k*-space by the larger *k*'s, the small concentration of large *k*'s in the back-projection method can lead to the loss of finer details of the sample (*9*). We can therefore conclude that under these conditions, for a similar voxel size, the physical resolution of the FI method is superior in comparison with the FBP method.

To examine our resolution limit, we define a simplified measure of signal to noise ratio, *S*/*N*, in our images. We define *S* as the maximal signal in the sample, and *N* as the rms value

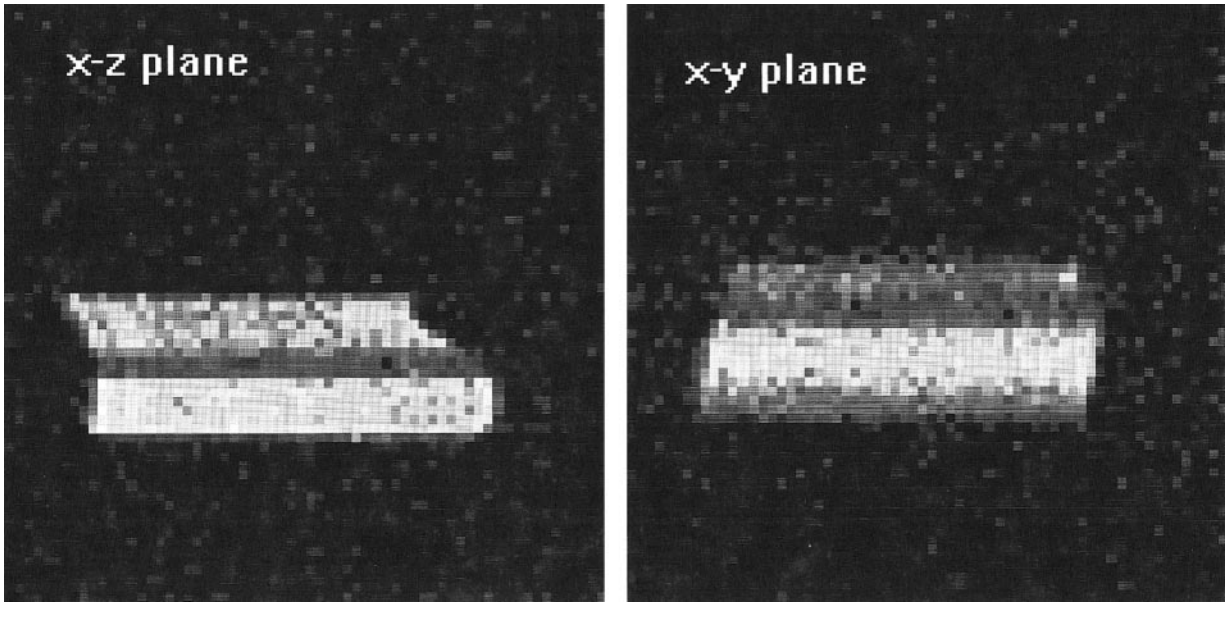

FIG. 3. Slices of the *x*-*z* and *x*-*y* planes reconstructed from the data used in Fig. 1.

of voxels in a typical area outside the sample. Thus defined we calculated $S/N = 14 \pm 1$ for the images with 30 μm^3 voxels presented in Figs. 2 and 3. The relation between voxel size and total acquisition time for the same signal-to-noise in 3D FI is given by $t \propto (\Delta x)^6$ (*8*), implying that to achieve the same signal-to-noise for a voxel size of 15 μm^3, under the present conditions, we would need an acquisition time of 96 h. In Fig. 5 we present an actually confirmed resolution of 20 μm^3 obtained by a 12-h measurement (a bit less than the 17 h required theoretically), indicating that after optimization 15 μm^3 would be a practical resolution limit.

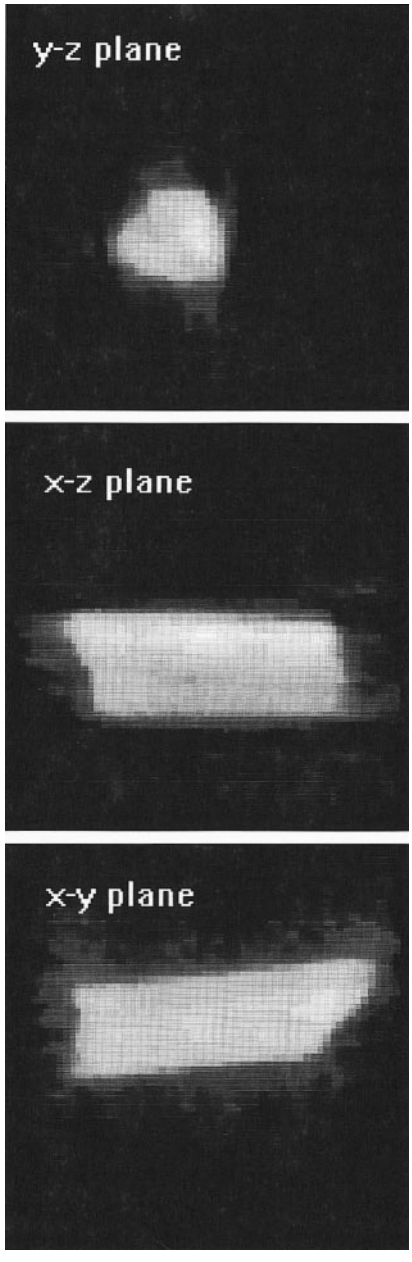

FIG. 4. Slices of the *y-z*, *x-y*, and *x-z* planes from the sample presented previously, obtained using the 3D filtered back-projection method. Voxel size and fov are approximately the same.

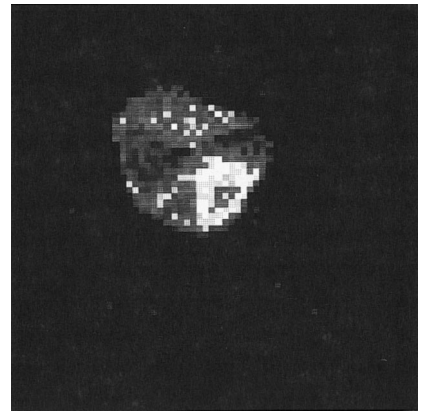

FIG. 5. A slice of the *y-z* plane from the same sample reconstructed from 3D FI acquisition data, with a voxel size of 20 μm^3.

In conclusion, we have demonstrated in the present Communication that 3D spin-warp Fourier imaging of conduction electrons in 1D organic crystals is a viable technique for spins with T2 values in the microsecond range. These values can be found in $(FA)_2PF_6$ and $(PE)_2PF_6$ (*2*) crystals and potentially in other 1D organic crystals. The maps presented in this Communication are spin density maps of the conduction electrons. Further experiments can be performed to obtain T2 maps and diffusion contrast maps. The FI method enables good separation between different spatial directions, which is necessary in order to study the conduction anisotropy in flouranthene and in other organic conductors.

ACKNOWLEDGMENTS

This research was supported by a grant from the German–Israeli Foundation for Scientific Research and Development.

REFERENCES

1. A. Coy, N. Kaplan, and P. T. Callaghan, *J. Magn. Reson. A* **121,** 201 (1996).
2. T. Wokrina, E. Dormann, and N. Kaplan, *Phys. Rev. B* **54,** 10492 (1996).
3. P. T. Callaghan, A. Coy, R. Ruf, E. Dormann, and N. Kaplan, *J. Magn. Reson. A* **111,** 127 (1994).
4. M. Conradi, A. N. Garroway, D. G. Cory, and J. Miller, *J. Magn. Reson.* **94,** 370 (1991).
5. A. Kumar, D. Welti, and R. R. Ernst, *J. Magn. Reson.* **18,** 69 (1975).
6. J. E. Tanner and E. O. Stejskal, *J. Chem. Phys.* **49,** 1768 (1968).
7. G. Mcgibney, M. R. Smith, S. T. Nichols, and A. Crawley, *Magn. Reson. Imaging* **30,** 51 (1993).
8. P. Mansfield and P. G. Morris, "NMR Imaging in Biomedicine," Academic Press, New York (1982).
9. P. T. Callaghan, "Principles of Nuclear Magnetic Resonance Microscopy," Oxford Univ. Press, Oxford (1991).